Progress In Electromagnetics Research, Vol. 138, 499–518, 2013

EFFECTIVE RECONSTRUCTION OF THE ROTATION-INDUCED MICRO-DOPPLER FROM A NOISE-CORRUPTED SIGNATURE

Ji-Hoon Park* **and Noh-Hoon Myung**

Department of Electrical Engineering, Korea Advanced Institute of Science and Technology (KAIST), 335 Gwahangno, Yuseong-gu, Daejeon 305-701, Korea

Abstract—This paper presents an effective method for reconstructing the rotation-induced micro-Doppler from a signature corrupted by noise. Based on empirical mode decomposition (EMD), a low-pass filter is employed as its preprocessor in order to effectively extract the first chopping harmonic component of the rotation-induced micro-Doppler. Then the extracted component is used for reconstructing the original micro-Doppler signature in the joint time-frequency domain. Although it is difficult to interpret the time-frequency representation of the noise-corrupted signature, the reconstruction of the micro-Doppler enables the acquisition of related information and can be used for complementing other traditional analysis methods. By validating the applicability of the proposed method with measured jet engine modulation (JEM) signatures, we demonstrate that the reconstruction process presented in this paper is expected to be significantly helpful for radar target recongnition in real environments.

1. INTRODUCTION

It is well-known that an aircraft target with a rotating propeller generates a rotation-induced micro-Doppler phenomenon [1–3], which is different from the Doppler shift caused by bulk translational motion [4, 5]. The frequency of the radar signature modulated by the rotational micromotion has periodic characteristics and reflects the detailed structure of the rotating part. Thus, the rotation-induced micro-Doppler effect has been widely applied in radar target recognition along with 1D rang profiles, synthetic aperture radar

Received 20 February 2013, Accepted 25 March 2013, Scheduled 3 April 2013

* Corresponding author: Ji-Hoon Park (dydynoel@kaist.ac.kr).

(SAR) images and ISAR (inverse SAR) images [6–13]. For analyzing the rotation-induced micro-Doppler, various analysis methods have been adopted to acquire useful information, such as the rotation rate and the number of blades. Traditionally, the time-domain methods, such as auto-correlation and cepstrum, have been used for estimating the fundamental periodicity [14–16]. The frequency spectrum has been commonly used for observing dominant spectral components that represent the blade chopping harmonics [16]. In recent years, time-frequency analysis techniques have been employed to complement these single-domain methods. Previous studies demonstrated that time-frequency analysis techniques clearly represented the time-dependent characteristics of a variety of micro-Doppler phenomena [17–24]. In particular, they could give physical insight into the periodic characteristic of rotation-induced micro-Doppler in the joint time-frequency domain [20–24].

However, most studies associated with the time-frequency analysis of the rotation-induced micro-Doppler have put less emphasis on the noise effect, which can deteriorate the original signature. When the micro-Doppler is affected by substantial noise, there is a high probability that the proper time-dependent characteristics cannot be observed in the joint time-frequency domain [23, 24]. Thus the time-frequency analysis becomes no longer valid in complementing other traditional analysis methods. To mitigate this problem an infinite impulse response (IIR) filter combined with the short-time Fourier transform (STFT) was employed in [23] to filter out spectral components higher than the first chopping harmonic. However, this approach is limited since the STFT essentially cannot discriminate between the micro-Doppler component and noise. In [24], empirical mode decomposition (EMD) [25] preprocessed by wavelet decomposition was used to extract the micro-Doppler component with reduction of the noise effect. However, this approach still meets difficulties in practical applications since the wavelet operation only allocates the signal spectrum into fixed spectral ranges.

In this paper, we propose a more effective method with an approach of further improving EMD to focus on the rotation-induced first chopping harmonic. According to previous studies [26, 27], EMD functioned as an adaptive filter bank with different pass-bands. Therefore, a preprocessor for supplementing the EMD should be developed based on this inherent characteristic. This paper employs EMD combined with a low-pass filter (LPF) for better applicability in practical cases. Since the cutoff frequency of the LPF is adaptively determined by the detected fundamental chopping frequency, the additional filtering operation can help the EMD

cover the appropriate spectral range of the first chopping harmonic component. As a result, the modified EMD extracts the intrinsic mode function (IMF) containing this component more effectively than the original EMD. Using the extracted IMF, the rotation-induced micro-Doppler is analyzed using two time-frequency analysis techniques, the Hilbert spectrum and the smoothed pseudo Wigner-Ville distribution (SPWVD).

The remainder of this paper is organized as follows. Section 2 presents the proposed reconstruction method and illustrates its application. In Section 3, signatures measured from a jet engine model are examined to validate the applicability of the proposed method. Finally, summary and conclusions are drawn in Section 4.

2. PROPOSED RECONSTRUCTION METHOD AND ITS APPLICATION EXAMPLE

When the rotation-induced micro-Doppler is influenced by noise, the first chopping harmonic containing the micro-Doppler component is more likely to be detected than other higher-order chopping harmonics. This harmonic can be identified via conventional spectral analysis and has provided information on the fundamental chopping frequency, which indicates the rate of a propeller blade moving to its adjacent position. Hence, for reconstructing the rotation-induced micro-Doppler from a noise-corrupted signature, it is important to effectively extract this component. Although there can be several ways for extraction, a data-driven method needs to be exploited to deal with various cases of noise corruption. In this respect, EMD is an excellent data-driven method since it operates as an adaptive time-varying filtering algorithm based on the intrinsic characteristic of the given signature [28–30]. Therefore, in this paper, the first chopping harmonic component is chiefly focused and EMD is considered as an extraction method.

2.1. Proposed Method for Reconstructing Rotation-induced Micro-Doppler

EMD, which was first proposed in [25], is a well-known method for processing signals with non-linear and non-stationary characteristics. It iteratively decomposes a signal into a finite number of IMFs that have the same number of zero crossings as that of extrema and simultaneously have symmetric envelopes determined by local maxima and local minima, respectively. These resultant IMFs denote respective modes consisting of the signal. Because of its empirical and data-driven

nature, EMD can be considered as a promising tool for handling noise-corrupted signatures. However, according to the intrinsic property of EMD reported in [26], EMD is composed of iterative sifting processes and equivalently functions as a filter bank (group) where the filter of number $k+1$ roughly occupies the half-band of the previous filter of number k. In order to gain insight into this property, the IMFs extracted by applying EMD to white Gaussian noise are shown in Fig. 1. From the frequency response of IMF 1 (the first extracted IMF), it is seen that the EMD filter of number 1 ($k=1$) corresponds to a high-pass filter. Other EMD filters of numbers greater than 1 are expressed by overlapping band-pass filters. By this characteristic, there can be two problems related to rotation-induced micro-Doppler analysis with EMD. First, it is desirable for each IMF not to have multiple frequency components [24, 27, 31] since the IMFs should denote the individual modes consisting of the original signal. Nevertheless, the EMD filter of a small number can fail to capture the mono-frequency component by its relatively wide pass-band. Second, from the relations of the EMD filters when $k > 1$, the center frequencies of these 'band-pass type' EMD filters may not be coincident with the frequency of interest, i.e., the fundamental chopping frequency. Hence, any EMD filters cannot completely include the micro-Doppler component in this case.

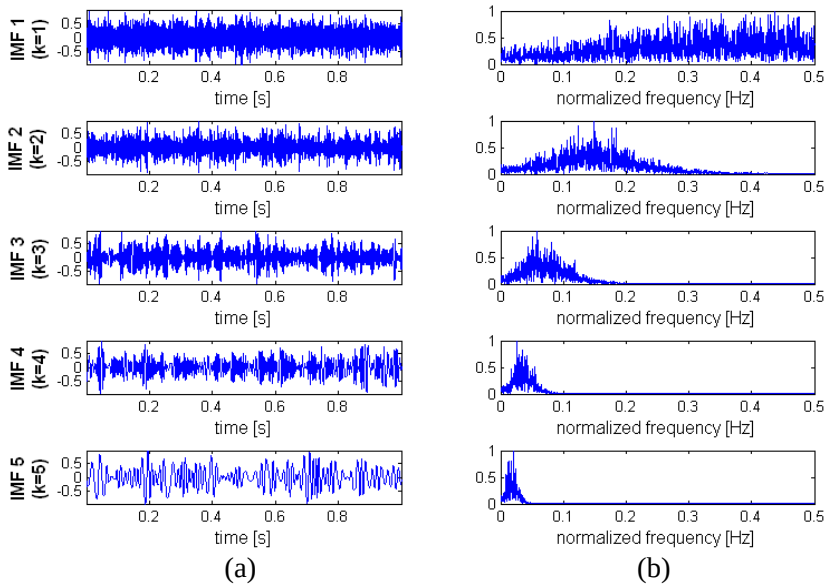

Figure 1. EMD operation to white Gaussian noise ((a) time domain, (b) frequency domain) [26].

Because of these problems in EMD, it can be difficult to clearly determine the IMF that contains the first chopping harmonic component. Fig. 2(a) shows the conceptual EMD operation to the rotation-induced micro-Doppler spectrum to illustrate EMD failure. In Fig. 2(a), the EMD filters of numbers 2 and 3 include the first chopping harmonic component. However, IMF 2 extracted from the EMD filter of number 2 cannot be considered since it causes the 'first' problem of the EMD application. Even though IMF 3 has a more compact spectral region than IMF 2, the first chopping harmonic component cannot be effectively captured in the EMD filter of number 3 by the 'second' problem. Consequently, the original EMD is limited to being employed in the sense that the extraction of the first chopping harmonic plays an important role in the reconstruction.

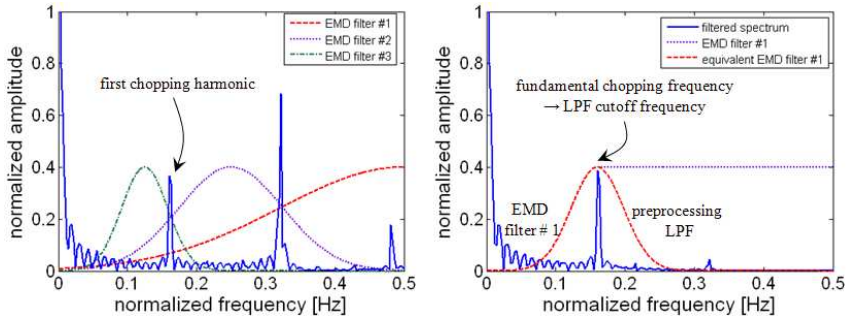

Figure 2. Conceptual EMD operation to the rotation-induced micro-Doppler spectrum: (a) original EMD operation and (b) modified EMD operation to the filtered spectrum.

To supplement the original EMD, the LPF whose cutoff frequency is selected as the detected fundamental chopping frequency is inserted as a preprocessor. Due to the preprocessing filtering, the first chopping harmonic component is automatically assigned to the EMD filter of number 1, and IMF 1 can have the center frequency in accordance with the cutoff frequency. This means that the IMF containing the micro-Doppler component is directly determined as IMF 1 without spectrum comparison between the original signature and IMFs [17, 31]. Since the EMD filter of number 1 operates as a high-pass filter, EMD combined with the LPF equivalently behaves like a band-pass filter with the center frequency same as the fundamental chopping frequency as shown in Fig. 2(b). Therefore, the LPF is expected to help EMD cover an accurate spectral range of the first chopping harmonic. In addition, the noise effect can significantly decrease since the two consecutive

steps also filter out the noise components. The rotation-induced micro-Doppler signature is then analyzed by applying time-frequency analysis techniques to the extracted IMF 1.

This paper employs the Hilbert spectrum and the SPWVD as the time-frequency analysis techniques to analyze the rotation-induced micro-Doppler in the joint time-frequency domain. The Hilbert spectrum calculates the instantaneous frequency by taking the time derivative of the phase $\Phi(t)$ derived from the IMF as follows:

$$f_D(t) = \frac{1}{2\pi}\frac{d\Phi(t)}{dt} \tag{1}$$

Application of the Hilbert spectrum becomes valid when the examined signal is close to the mono-frequency function. Thus, the resultant Hilbert spectrum approximately shows a single-mode sinusoidal waveform indicating the time-dependent characteristic of the extracted component [24, 27, 31]. By estimating the exhibited time period, it is possible to check if IMF 1 retains the appropriate time-varying characteristic.

The SPWVD is the representative of Cohen's class and is a compromise between the cross-interference problem and the high-resolution advantage of the original Wigner-Ville distribution (WVD). For a signal $x(t)$, the mathematical expression of the SPWVD is given by

$$\begin{aligned}&\mathrm{SPWVD}_x(t,f)\\ &= \int_{-\infty}^{\infty} g(\tau) \int_{-\infty}^{\infty} h(\nu-t)x(\nu+\tau/2)x^*(\nu-\tau/2)d\nu \exp(-j2\pi f\tau)d\tau\end{aligned} \tag{2}$$

where $g(\cdot)$ and $h(\cdot)$ are the time smoothing function and the frequency smoothing function, respectively. Note that the lengths of smoothing functions should be much shorter than one cycle of the modulation frequency to produce an accurate instantaneous Doppler frequency [17, 32]. The resolution of the SPWVD may be restricted to visualizing the weakly-modulated micro-Doppler [17]. However, since the propeller blade length is generally larger than the radar wavelength λ, the SPWVD is sufficient for representing the rotation-induced micro-Doppler [3]. The SPWVD can yield the complete time-frequency representation of the rotation-induced micro-Doppler by directly applying it to extracted IMF 1. As described above, the proposed method can have good applicability. In addition, it is easy to handle because the extraction process, the most important part of reconstruction, only introduces additional low-pass filtering to the existing EMD method. The overall procedures are described in Fig. 3.

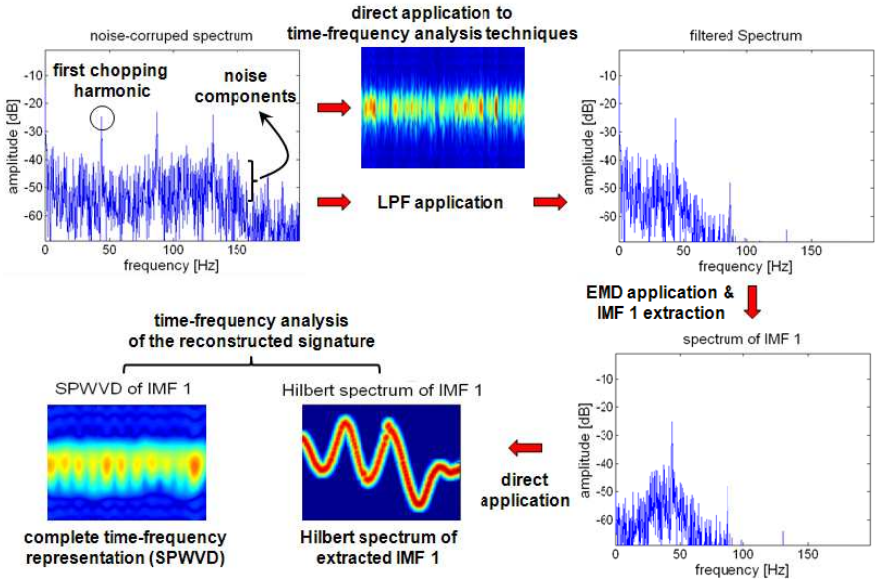

Figure 3. Overall procedures for reconstructing the rotation-induced micro-Doppler affected by noise.

2.2. Illustrative Application Example with a Simple Rotation-induced Micro-Doppler

For examining the proposed reconstruction method, we describe an illustrative example with a simple micro-Doppler signature [33]. As shown in Fig. 4(a), a propeller blade is modeled as a rectangular PEC flat plate with a size of $L_1 \times L_2$. The blade is located with the fixed skew angle Φ_s and rotates with the time-varying angle θ_s. (x, y, z) and (x', y', z') are the global coordinate system and the local coordinate system with respect to the blade, respectively. To obtain the high-frequency scattered field, the fictitiously induced equivalent electric and magnetic currents [33–36] are calculated along each blade edge. With the potential theory and the quasi-stationary approach, the radiation integral of the equivalent currents yields a time-varying scattered field. The single blade model is extended to the propeller with 4 blades by compensating for the translation of each blade as shown in Fig. 4(b). Table 1 summarizes the parameters related to the simulation. The incident angle Ψ denotes the angle between the direction of the incident plane wave and the axis of rotation (y-axis in Fig. 4). Because there are 4 blades, the theoretical fundamental chopping frequency is 40 Hz, which is chosen as the cutoff frequency of

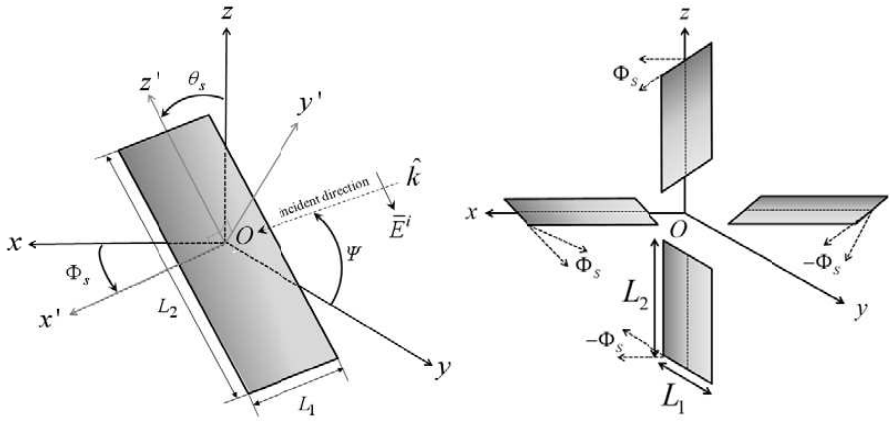

Figure 4. (a) A propeller blade modeled as a PEC flat plate and (b) analysis model extended to a propeller.

Table 1. Parameters related to the simulation for a sufficiently short wavelength λ.

number of samples per sec.	3600
polarization	$\theta\theta$-polarization
incident angle (Ψ), skew angle (Φ_s)	90°, 10°
rotation frequency (f_r)	1 Hz (600 RPM)
blade lengths (L_1, L_2)	2λ, 5λ
number of blades	4

the preprocessing LPF. The elliptic type filter is employed as the kind of the LPF in this simulation.

Figure 5(a) depicts the SPWVD result of the simulated signature. Figs. 5(b) and (c) show the extracted first chopping harmonic component in the Hilbert spectra normalized to the properly chosen scaling factor. These two Hilbert spectra resulted from the EMD combined with the LPF and the original EMD, respectively. The SPWVD result in Fig. 5(a) reveals the typical time-frequency representation of the rotating propeller [3, 21, 22]. As explained above, the Hilbert spectrum of IMF 1 in Fig. 5(b) exhibits the waveform characterized by the single sinusoid varying with the chopping rate. Fig. 5(c) shows the Hilbert spectrum of IMF 3, which corresponds to the first chopping harmonic component extracted from the original

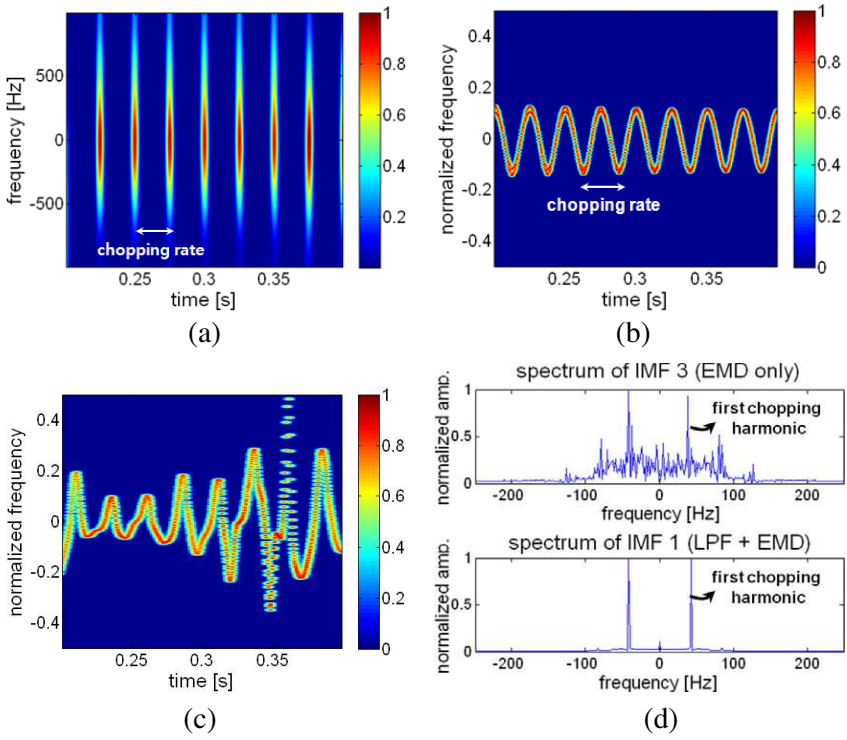

Figure 5. (a) SPWVD result of simulated rotation-induced micro-Doppler signature, (b) Hilbert spectrum of IMF 1 from the EMD combined with the LPF, (c) Hilbert spectrum of IMF 3 from the original EMD and (d) comparison between the spectrum of IMF 3 (EMD only) and that of IMF 1 (LPF + EMD).

EMD. Compared with Fig. 5(b), Fig. 5(c) shows the distorted and irregular waveform. As illustrated in Fig. 5(d), IMF 3 fails to accurately capture the first chopping harmonic component. In contrast, IMF 1 obviously shows the fact that the LPF effectively supplements the original EMD.

In this micro-Doppler simulation, the noise components were not considered. Hence, direct application of conventional time-frequency techniques, such as the SPWVD and the STFT is suitable for analyzing the micro-Doppler in the joint time-frequency domain. To further develop the discussion on the micro-Doppler signature highly contaminated by noise, additive white Gaussian noise (AWGN) is added to the simulated signature to make a peak-power signal-to-noise ratio (peak-power SNR) of 5 dB. Note that the peak-power SNR [1]

with respect to the first chopping harmonic is given by

$$\mathrm{SNR}_{\mathrm{peak}} = \frac{P_{\mathrm{peak}}}{\sigma^2} \tag{3}$$

where P_{peak} is the power of the spectral peak and σ^2 the Gaussian noise variance. When the peak-power SNR becomes 0 dB, the first chopping harmonic will not be observed, and thus it is difficult for the proposed method to work properly.

Figure 6 illustrates the SPWVD result of the noise-corrupted signature and the Hilbert spectrum of the extracted IMF 1. The SPWVD result shows such a smeared waveform that any useful information cannot be obtained. In contrast, the Hilbert spectrum still reveals a sinusoidal waveform even though it is slightly distorted by residual noise. In Fig. 7, the rotation-induced micro-Doppler is reconstructed and represented in the joint time-frequency domain by applying the SPWVD to the IMF 1. Different from the SPWVD result of the raw signature, the resultant waveform in Fig. 7(a) exhibits significantly improved time-frequency localization. We choose the maximum Doppler frequency shift $f_{D,\max}$ as the frequency value with an amplitude (energy distributed in the time-frequency plot) of approximately 30% of the maximum amplitude where the distinct contour of the sinusoidal curve induced by the blade tip can be observed. Using the estimated value, the blade length L_2, which mainly contributes to $f_{D,\max}$, can be estimated as follows [2, 22–24]:

$$L_2 = \frac{\lambda f_{D,\max}}{4\pi f_r \sin\psi} \tag{4}$$

Here, the blade length estimated from Fig. 7(b) shows a good match with the theoretical value of 5λ.

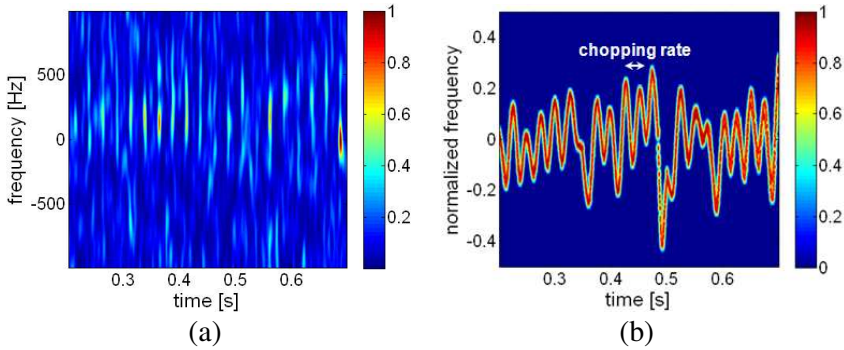

Figure 6. (a) SPWVD result of noise-corrupted signature and (b) Hilbert spectrum of the extracted IMF 1.

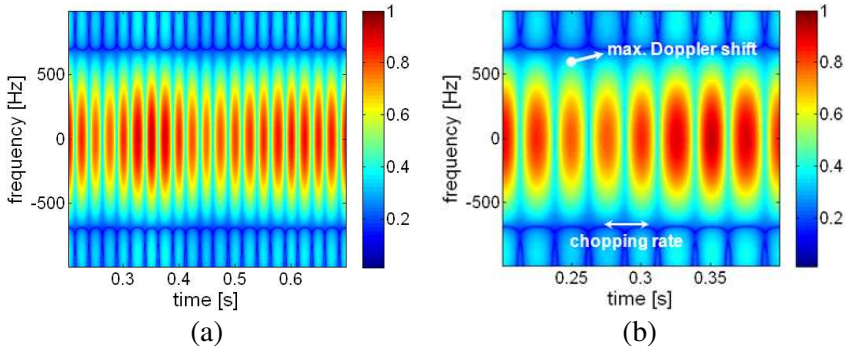

Figure 7. (a) SPWVD result of the extracted IMF 1 and (b) expanded SPWVD result related to (a).

The simulation study presented in this section demonstrates that the proposed method has an excellent performance for reconstructing the rotation-induced micro-Doppler from the noise-corrupted signature.

3. APPLICATION OF PROPOSED RECONSTRUCTION METHOD TO MEASURED JEM SIGNATURES

The JEM effect is a representative rotation-induced micro-Doppler phenomenon generated by the rotating engine compressor. Since the JEM undergoes a large amount of scattering, the outstanding chopping harmonics of the actual JEM spectrum can be affected not only by environmental noise but also by the inter-modulation effect between rotating blades equipped in different rotor stages. In order to acquire realistic JEM signatures, an experimental jet engine model was fabricated in [37]. Complete CAD model of the engine structure and its photograph are shown in Fig. 8. The information on the engine model and relevant measurement parameters are given in Table 2. In [23, 24], the raw measured JEM signatures were contaminated by noise components, and thus no meaningful parameters could be extracted in the joint time-frequency domain.

In order to correct this problem, we applied the proposed method to the measured JEM signatures. The JEM chopping harmonics generated by the first rotor stage of the engine are chiefly concentrated because the rotation of this stage primarily contributes to the JEM effect in practical cases [14–16]. Therefore, in this paper, other spectral components were equated with noise components. Fig. 9 shows the JEM power spectra for two different rotation speeds, 180.7 RPM

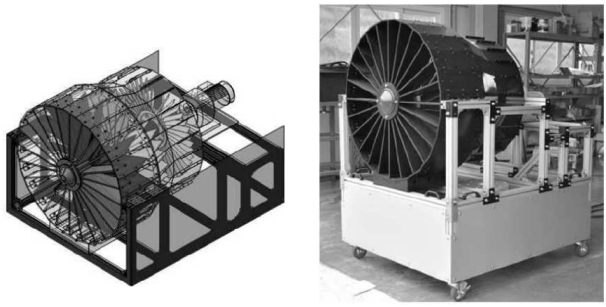

(a) (b)

Figure 8. Fabricated jet engine model: (a) complete CAD and (b) photograph (referred from [36]).

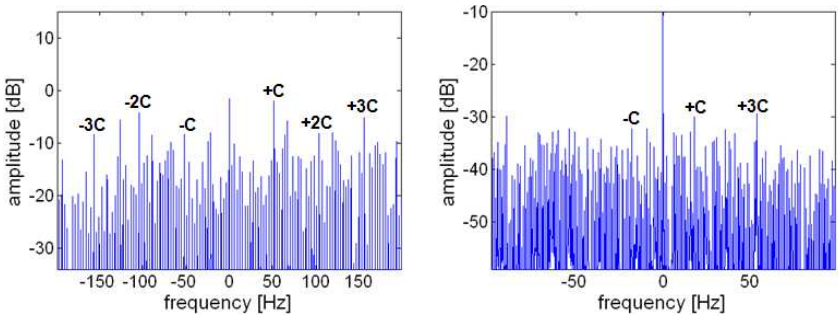

Figure 9. JEM power spectra at the rotation speeds of (a) 180.7 RPM and (b) 60.1 RPM.

Table 2. Information on the experimental engine model and relevant measurement parameters.

stage number	1	2	3
number of blades	17	29	41
length of each blade	0.385 m	0.325 m	0.300 m
radar carrier frequency	10 GHz		
pulse repetition frequency (PRF)	1.8 kHz		
rotation speed	180.7 RPM, 60.1 RPM		
incident angle	50°		

and 60.1 RPM. The JEM chopping harmonics are observed from respective spectra and are marked as 'xC'. The preceding number 'x' denotes the harmonic order and is omitted for the first chopping harmonic. From two exhibited power spectra, the peak-power SNR values are estimated as 11.3 dB and 4.2 dB, respectively. The detected fundamental chopping frequencies of 51.6 Hz and 18.0 Hz are used for the cutoff frequencies of the preprocessing LPF.

Figure 10 depicts the spectra of IMFs extracted from the filtered JEM spectrum for a rotation speed of 180.7 RPM. As expected, IMF 1 contains the first chopping harmonic component. From the Hilbert spectrum of IMF 1 in Fig. 11, the chopping rate can be estimated using the exhibited time-dependent waveform. It is clear that the modified EMD operation effectively extracts the first chopping harmonic component from the measured JEM signature. Furthermore, the spool rate indicating one revolution period can be found from a partially repeating group as denoted in Fig. 11. This is due to the fact that the spool rate gives the fundamental periodicity to the JEM signature, whose mathematical model [14] is given by

$$s_{\mathrm{JEM}}(t) = \left\{ \sum_{n=-\infty}^{\infty} a_n e^{j2\pi n f_r t} \right\} e^{j \sum_{n=-\infty}^{\infty} \beta_n \sin(2\pi f_r n t)} e^{j2\pi f_0 t} \tag{5}$$

Here, the first and the second term denote the amplitude modulation and the phase modulation, respectively. For the index of n, a_n and β_n

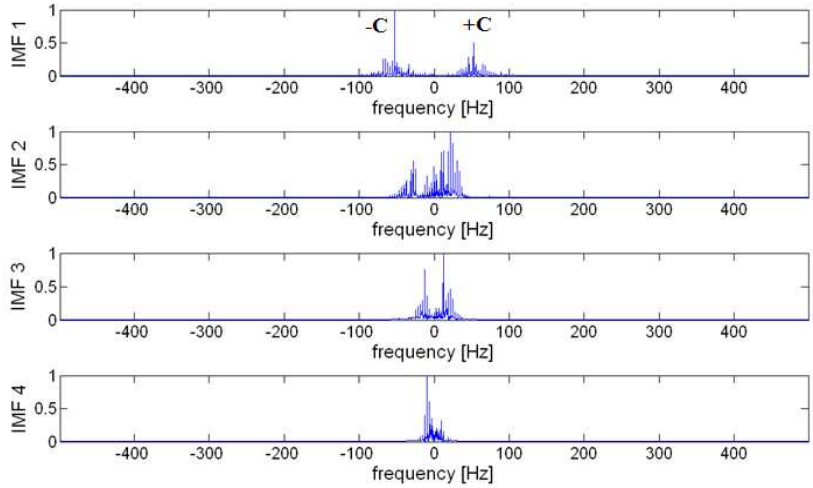

Figure 10. IMFs after applying the EMD to the filtered JEM spectrum for a rotation speed of 180.7 RPM.

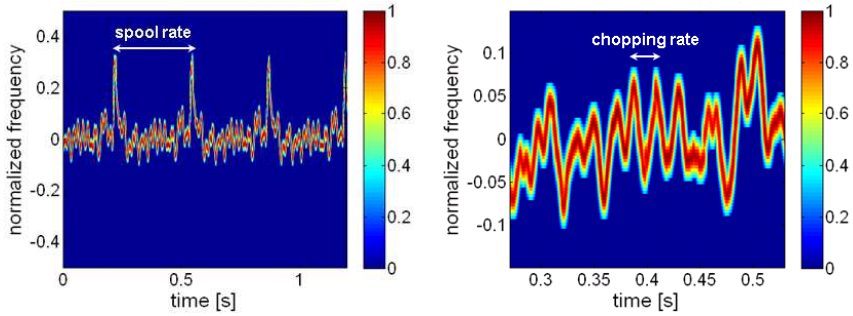

Figure 11. (a) Hilbert spectrum of the extracted IMF 1 for the jet engine model rotating at the rate of 180.7 RPM and (b) expanded Hilbert spectrum related to (a).

are the Fourier series coefficients. f_0 is the radar carrier frequency and f_r is the rotation frequency, the reciprocal of the spool rate. As shown in Fig. 10, the extracted IMF 1 includes not only the first chopping harmonic but also the spool line spectra around the center frequency. As a result, the Hilbert spectrum of IMF 1 can provide information on the number of blades using the chopping rate and the spool rate marked in Fig. 11(b). In addition, the Hilbert spectrum is also interpreted as approximately showing the time-dependent characteristic of the first chopping harmonic component and surrounding spool line spectra, which can be derived from the PM part of (4) as follows:

$$f(t) = f_r \sum_{n=N-a}^{N+a} \beta_n n \cos(2\pi f_r n t) \tag{6}$$

where $2a$ is the number of spool line spectra included in IMF 1 and N the number of blades equipped in the first rotor stage. The SPWVD is then applied to IMF 1 and the result is shown in Fig. 12. In contrast to the SPWVD result of the raw measured JEM signature in Fig. 13, useful information can now be obtained from the well-presented time-frequency localization. Apart from the chopping rate, it is possible to calculate the blade length from the maximum Doppler frequency shift. Even if other effects, such as residual noise or the jet engine cavity effect, can lead to some errors in calculation, the estimated blade length gives a reasonable value in relation to the real blade length of the first rotor stage. Note that the lengths of the smoothing functions were chosen as $g = 6.0\,\text{ms}$ and $h = 5.0\,\text{ms}$ for sufficient time-frequency resolution.

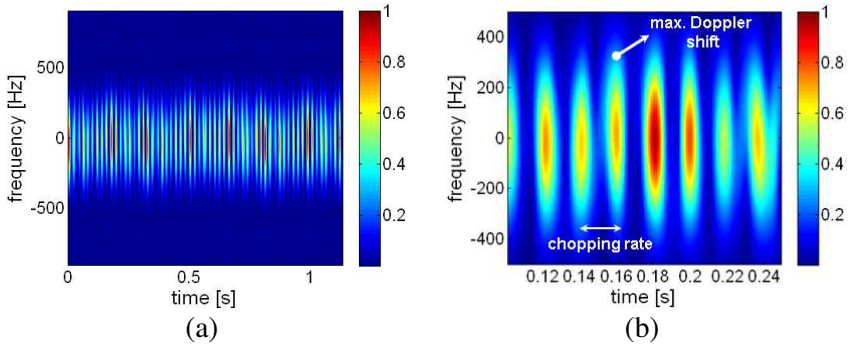

Figure 12. Reconstruction of the JEM micro-Doppler (180.7 RPM): (a) SPWVD result of the extracted IMF 1 and (b) expanded SPWVD result related to (a).

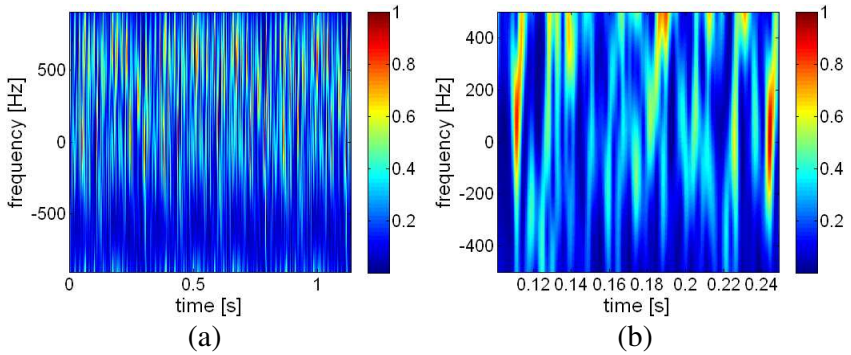

Figure 13. (a) SPWVD result of the raw measured JEM signature and (b) expanded SPWVD result related to (a).

Figure 14 shows the case when the rotation speed decreases to 60.1 RPM. Although the SPWVD result in Fig. 14(a) shows an irregular waveform by noise components, the Hilbert spectrum of the extracted IMF 1 in Fig. 14(b) indicates that the JEM first chopping harmonic component is appropriately captured by the EMD combined with the LPF. The SPWVD result of IMF 1 in Fig.14(c) exhibits a much clearer waveform than the result in Fig. 14(a). In this case, the lengths of smoothing functions were given as $g = 12.0\,\text{ms}$, $h = 8.0\,\text{ms}$, respectively. On account of the decreased rotation speed, the related parameters, such as the maximum Doppler frequency shift are diminished [16]. The reconstructed micro-Doppler can be analyzed in a similar way.

In this section, the rotation-induced JEM signature corrupted

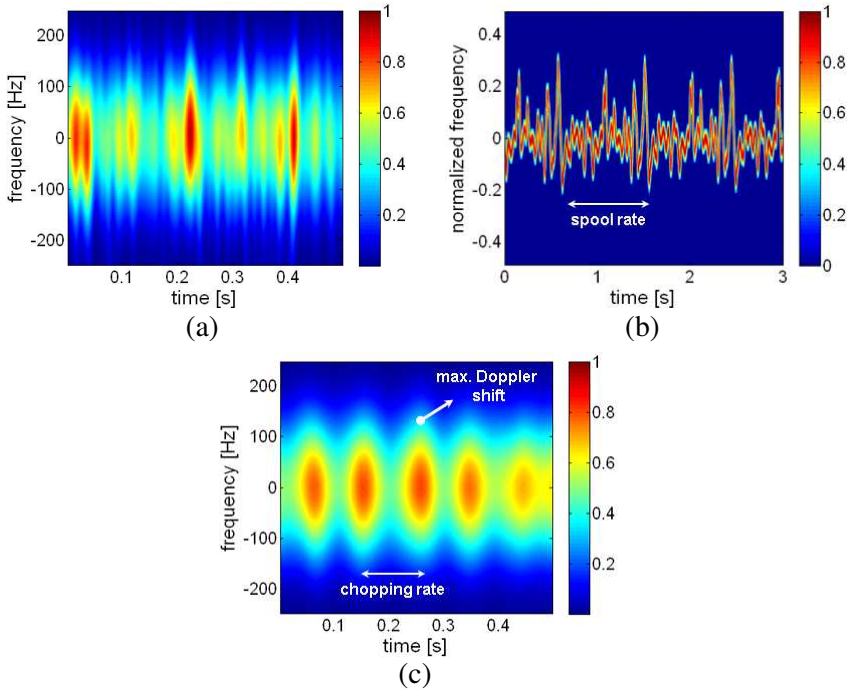

Figure 14. Case when the rotation speed decreases to 60.1 RPM: (a) expanded SPWVD result of the raw measured JEM signature, (b) Hilbert spectrum of the extracted IMF 1 and (c) expanded SPWVD result of the extracted IMF 1.

by noise components was effectively reconstructed via the proposed method. Although some irregularity was still observed, the refined time-frequency representations enabled us to obtain useful information on the rotating jet engine. The developed reconstruction process also demonstrated that it could be used for various cases with different rotation speeds. Thus, time-frequency analysis became valid in complementing other traditional methods for noise-corrupted signatures.

4. CONCLUSION

This paper presented the effective reconstruction of the rotation-induced micro-Doppler from a noise-corrupted signature. The application of the EMD combined with the adpative LPF effectively extracted IMF 1 containing the first chopping harmonic component.

The Hilbert spectrum of IMF 1 showed the time-dependent characteristic of the extracted component embedded in the noise-corrupted signature. The SPWVD result could reveal the refined time-frequency representation of the rotation-induced micro-Doppler. The application to the measured JEM signatures demonstrated that the proposed method had good applicability to real micro-Doppler signatures. The reconstruction described in this paper is appropriate for micro-Doppler analysis in real environments where noise components can degrade the original signal component. Furthermore, it will likely facilitate more accurate radar target recognition by complementing other traditional analysis methods.

ACKNOWLEDGMENT

This research was supported by Samsung Thales Co., Ltd.

REFERENCES

1. Chen, V. C. and H. Ling, *Time-frequency Transforms for Radar Imaging and Signal Analysis*, Ch. 8, Artech House, Norwood, MA, 2002.
2. Chen, V. C, F. Li, S. S. Ho, and H. Wechsler, "Micro Doppler effect in radar: Phenomenon, model and simulation study," *IEEE Trans. on Aerospace and Electronic Systems*, Vol. 42, No. 1, 2–21, 2006.
3. Chen, V. C., W. Miceli, and B. Himed, "Micro-Doppler analysis in ISAR — Review and perspectives," *Int. Radar Conf. — Surveillance for a Safer World*, 1–6, 2009.
4. Qi, C., Z. Zhao, W. Yang, Z. Nie, and G. Chen, "Electromagnetic scattering and Doppler analysis of three-dimensional breaking wave crests at low-grazing angles," *Progress In Electromagnetics Research*, Vol. 119, 239–252, 2011.
5. Nie, D., M. Zhang, X. Geng, and P. Zhou, "Investigation on Doppler spectral characteristics of electromagnetic backscattered echoes from dynamic nonlinear surfaces of finite-depth sea," *Progress In Electromagnetics Research*, Vol. 130, 169–186, 2012.
6. Chang, Y. L., C. Y. Chiang, and K. S. Chen, "SAR image simulation with application to target recognition," *Progress In Electromagnetics Research*, Vol. 119, 35–57, 2011.
7. Zhang, M., Y. W. Zhao, H. Chen, and W. Q. Jiang, "SAR imaging simulation for composite model of ship on dynamic ocean scene," *Progress In Electromagnetics Research*, Vol. 113, 395–412, 2011.

8. Wu. J., Z. Li, Y. Huang, Q. H. Liu, and J. Yang, "Processing one-stationary bistatic SAR data using inverse scaled Fourier transform," *Progress In Electromagnetics Research*, Vol. 129, 143–159, 2012.
9. Yang, W., Y. Liu, G. S. Xia, and X. Xu, "Statistical mid-level features for building-up area extraction from full polarimetric SAR imagery," *Progress In Electromagnetics Research*, Vol. 132, 233–254, 2012.
10. Buddendick, H. and T. F. Eibert, "Bistatic image formation from shooting and bouncing rays simulated current distributions," *Progress In Electromagnetics Research*, Vol. 119, 1–19, 2011.
11. Calvo-Gallego, J. and F. Pérez-Martínez, "Simple traffic surveillance system based on range-Doppler radar images," *Progress In Electromagnetics Research*, Vol. 125, 343–364, 2012.
12. Park, S. H., J. H. Lee, and K. T. Kim, "Performance analysis of the scenario-based construction method for real target ISAR recognition," *Progress In Electromagnetics Research*, Vol. 128, 503–518, 2012.
13. Felguera-Martin, D., J. T. Gonzalez-Partida, and M. Burgos-Garcia, "Interferometric ISAR imaging on maritime target applications: Simulation of realistic targets and dynamics," *Progress In Electromagnetics Research*, Vol. 132, 571–586, 2012.
14. Bell, M. R. and R. A. Grubbs, "JEM modeling and measurement for radar target identification," *IEEE Trans. on Aerospace and Electronic Systems*, Vol. 29, No. 1, 73–87, 1993.
15. Cuomo, S., P. F. Pellegrini, and E. Piazza, "Model validation for 'jet engine modulation' phenomenon," *IEE Electronics Letters*, Vol. 30, 2073–2074, 1994.
16. Tait, P., *Introduction to Radar Target Recognition*, IET Radar, Sonar and Navigation Series 18, 2005.
17. Cai, C., W. Liu, J. S. Fu, and Y. Lu, "Radar micro-Doppler signature analysis with HHT," *IEEE Trans. on Aerospace and Electronic Systems*, Vol. 46, No. 2, 929–938, 2010.
18. Pan, X., W. Wang, J. Liu, D. J. Feng, Y. Liu, and G. Wang, "Features extraction of rotationally symmetric ballistic targets based on micro-Doppler," *Progress In Electromagnetics Research*, Vol. 137, 727–740, 2013.
19. Han, S. K., H. T. Kim, S. H. Park, and K. T. Kim, "Efficient radar target recognition using a combination of range profile and time-frequency analysis," *Progress In Electromagnetics Research*, Vol. 108, 131–140, 2010.

20. Thayaparan, T., S. Abrol, E. Riseborough, L. Stankovic, D. Lamothe, and G. Duff, "Analysis of radar micro-Doppler signatures from experimental helicopter and human data," *IET Radar Sonar and Navigation*, Vol. 1, 289–299, 2007.
21. Setlur, P., F. Ahmadn, and M. Amin, "Helicopter radar return analysis: Estimation and blade number selection," *Signal Processing*, Vol. 91, 1409–1424, 2011.
22. Pouliguen. P., L. Lucas, F. Muller, S. Quete, and C. Terret, "Calculation and analysis of electromagnetic scattering by helicopter rotating blades," *IEEE Trans. on Antennas and Propagation*, Vol. 50, 1396–1408, 2002.
23. Lim, H., J. H. Park, J. H. Yoo, C. H. Kim, K. I. Kwon, and N. H. Myung, "Joint time-frequency analysis of radar micro-Doppler signatures from aircraft engine models," *Journal of Electromagnetic Waves and Applications*, Vol. 25, Nos. 8–9, 1069–1080, 2011.
24. Park, J. H., H. Lim, and N. H. Myung, "Modified Hilbert-Huang transform and its application to measured micro Doppler signatures from realistic jet engine models," *Progress In Electromagnetics Research*, Vol. 126, 255–268, 2012.
25. Huang, N. E., Z. Shen, S. R. Long, M. C. Wu, H. H. Shih, Q. Zheng, N. C. Yen, C. C. Tung, and H. H. Liu, "The empirical mode decomposition and the Hilbert spectrum for nonlinear and non-stationary time series analysis," *Proc. of the Royal Society A*, Vol. 454, No. 1971, 679–699, 1998.
26. Flandrin, P., G. Rilling, and P. Gonçalvés, "Empirical mode decomposition as a filter bank," *IEEE Signal Processing Letters*, Vol. 11, 112–114, 2004.
27. Yinfeng, D., Y. Li, M. Xiao, and M. Lai, "Analysis of earthquake ground motions using an improved Hilbert-Huang transform," *Mechanical System and Signal Processing*, No. 22, 7–19, 2008.
28. Bai, X., M. Xing, F. Zhou, G. Lu, and Z. Bao, "Imaging of micromotion targets with rotating parts based on empirical mode decomposition," *IEEE Trans. Geoscience and Remote Sensing*, Vol. 46, No. 11, 3514–3523, 2008.
29. Yan, R. and R. X. Gao, "A tour of the Hilbert-Huang transform: An empirical tool for signal analysis," *IEEE Instrumentation and Measurement Magazine*, Vol. 10, No. 5, 40–45, 2007.
30. Mostafanezhad, I., O. Boric-Lubecke, V. Lubecke, and D. Mandic, "Application of empirical mode decomposition in removing fidgeting interference in Doppler radar life signs monitoring devices," *IEEE Engineering in Medicine and Biology*, Minneapolis, USA,

Sep. 2009.

31. Peng, Z. Z., P. Tse, and F. Chu, "An improved Hilbert-Huang transform and its application in vibration signal analysis," *Journal of Sound and Vibration*, No. 286, 187–205, 2005.
32. Sparr, T. and B. Krane, "Micro-Doppler analysis of vibrating targets in SAR," *IEE Radar Sonar and Navigation*, Vol. 150, 277–283, 2003.
33. Sun, Y. S. and N. H. Myung, "Analysis of electromagnetic scattering by a rotating rotor with flat blades," *Singapore ICCS'94*, Signapore, Nov. 1994.
34. McNamara, D. A., C. W. I. Pistorius, and J. A. G. Malherbe, *Introduction to the Uniform Geometrical Theory of Diffraction*, Ch. 7, Artech House, London, 1990.
35. Baussard, A., M. Rochdi, and A. Krenchaf, "PO/MEC-based scattering model for complex objects on a sea surface," *Progress In Electromagnetics Research*, Vol. 111, 229–251, 2011.
36. Garcia-Gonzalez, C., Y. Alvarez-Lopez, A. D. Casas, and F. Las-Heras, "Characterization of antenna interaction with scatterers by means of equivalent currents," *Progress In Electromagnetics Research*, Vol. 116, 185–202, 2011.
37. Lim, H., J. H. Yoo, C. H. Kim, K. I. Kwon, and N. H. Myung, "Radar cross section measurement of a realistic jet engine structure with rotating parts," *Journal of Electromagnetic Waves and Applications*, Vol. 25, No. 7, 999–108, 2011.